FINAL REPORT

Accelerating Use of Sustainable Materials in Transportation Infrastructure

Date: May 2016

Osman E. Ozbulut, Ph.D., Assistant Professor, University of Virginia
Zhangfan Jiang, Graduate Student, University of Virginia
Devin K. Harris, Ph.D., Assistant Professor, University of Virginia

Prepared by:

Department of Civil and Environmental Engineering
University of Virginia
351 McCormick Rd Thornton Hall
Charlottesville, VA 22904

Prepared for:
Virginia Center for Transportation Innovation and Research
530 Edgemont Road
Charlottesville, VA 22903

1. Report No.	2. Government Accession No.	3. Recipient's Catalog No.
4. Title and Subtitle Accelerating Use of Sustainable Materials in Transportation Infrastructure		**5. Report Date** **6. Performing Organization Code**
7. Author(s) Osman E. Ozbulut, Ph.D, Devin K. Harris, Ph.D		**8. Performing Organization Report No.**
9. Performing Organization Name and Address Department of Civil and Environmental Engineering University of Virginia 351 McCormick Rd Thornton Hall Charlottesville, VA 22904		**10. Work Unit No. (TRAIS** **11. Contract or Grant No.** DTRT13-G-UTC33
12. Sponsoring Agency Name and Address US Department of Transportation Office of the Secretary-Research UTC Program, RDT-30 1200 New Jersey Ave., SE Washington, DC 20590		**13. Type of Report and Period Covered** Final 6/01/15 – 5/24/16 **14. Sponsoring Agency Code**

15. Supplementary Notes

16. Abstract

With the push towards sustainable design of highway infrastructure systems owners have shown interest in leveraging materials with minimal environmental impacts and extended service lives. Within this emphasis most efforts on sustainable material design have focused on improving the durability of materials; however, an alternative trajectory for sustainable material design includes the development of materials with increased functionality to include features such as self-healing, self-cleaning, and self-sensing. This investigation focuses primarily on this last level of functionality within cementitious composites, such that concrete can be designed to function as a structural component, but with the added functionality of distributed sensing continuum. Over the past two decades, numerous research studies have been conducted to explore behavior of self-sensing cementitious composites with different functional fillers. Most of these studies investigated the use of fillers such as carbon nanofiber (CNF), carbon black, and carbon nanotubes (CNTs) in cement composites to develop a multifunctional material. More recently, graphene nanoplatelets (GNPs), which have very thin but wide aspect ratio, are drawing the graphene market due to their advantages such as ease of processing and excellent material properties at a very low cost. The application of two-dimensional GNPs in cementitious composites has yet to gain widespread attention. This report describes an investigation on the the self-sensing capabilities of GNP-reinforced hydraulic Portland cement composites. In particular, the effects of GNP content on the electrical properties and piezoresistive characteristics of mortar specimens are explored. In addition, a simple fabrication method that does not require special treating procedures such as ultrasonication and chemical (covalent) treatments for the dispersion of GNPs is pursued. The GNPs used in this study have an average thickness of 8 nanometers and a diameter of 25 microns. Standard prismatic mortar specimens containing different GNP concentrations were prepared using three different mixing procedures. The resistivity of the specimens was measured using a four-point probe method. Finally, the piezoresistive response of GNP-reinforced cement composites was evaluated under cyclic compressive loads. The GNP-reinforced mortar specimens exhibited good piezoresistive behavior under cyclic compressive loads when the GNP ratios exceed 5%.

17. Key Words	18. Distribution Statement
Self-sensing concrete, graphene nanoplatelets, strain sensing, piezoresistive	No restrictions. This document is available from the National Technical Information Service, Springfield, VA 22161

19. Security Classif. (of this report)	20. Security Classif. (of this page)	21. No. of Pages	22. Price
Unclassified	Unclassified	XX	

DISCLAIMER

The contents of this report reflect the views of the authors, who are responsible for the facts and the accuracy of the information presented herein. This document is disseminated under the sponsorship of the U.S. Department of Transportation's University Transportation Centers Program, in the interest of information exchange. The U.S. Government assumes no liability for the contents or use thereof.

TABLE OF CONTENTS

LIST OF FIGURES

LIST OF TABLES

PROBLEM

With the push towards sustainable design of highway infrastructure systems, the performance of construction materials has been at the center of this focus as owners seek leverage materials with minimal environmental impacts and extended service lives. Within this emphasis most efforts on sustainable material design have focused on improving the durability of materials such as steel and concrete to include features such as minimizing cracking, reduced permeability and porosity, greater resistance to freeze-thaw degradation, and mitigating corrosion potential. However, an alternative trajectory for sustainable material design includes the development of materials with increased functionality to include features such as self-healing, self-cleaning, and self-sensing.

Self-sensing cement-based composites have various advantages such as durability, compatibility with concrete matrix, and spatially distributed measurement capability over traditional strain sensors. Since early 1990s, numerous research studies have been conducted to explore the behavior of self-sensing cementitious composites with different functional fillers [1-3]. Most of these studies investigated the use of fillers such as carbon fiber (CF), carbon nanofiber (CNF), carbon black, and carbon nanotubes (CNTs) in cement pastes to develop a multifunctional composite. Galoa et al. [4] studied the self-sensing properties of carbon CNF reinforced cement pastes and tested prismatic specimens with different CNF dosages under compression. Similarly, Wen and Chung [5] tested small beam specimens made of cement pastes with short carbon fibers under flexural load. Chen and Liu [6] investigated the damage detection capabilities of cement pastes with micro-size carbon fibers.

Several researchers fabricated individual small-size cement sensors and embedded them into a structure. Xiao et al. [7] monitored the strain of the concrete columns under cyclic and monotonic loading using carbon black-filled cement based embedded sensors. Saafi [8] designed and fabricated a CNT-based cement sensor. The developed sensors with one electrode at each end were embedded into beam specimens and a wireless communication system was used to measure the response of the CNT-cement sensors. Azhari and Banthia [9] developed two cement-based sensors, one with carbon fibers alone and the other including both carbon fibers and CNTs. Under compressive loads, the response of the cement-based sensors found to be nonlinear and rate-dependent. They also indicated that the hybrid sensor provided a better quality signal, improved reliability and increased sensitivity over sensors carrying CF alone. D'Alessandro et al. [10] studied the comparative performance of self-sensing cementitious composites with CNT and CNF inclusions. The test results showed that CNF composite sensors have a higher level of noise and a greater influence of the polarization effect.

Recent advances in the development of graphene nanoplatelets (GNP), which have unique mechanical, thermal, and electrical properties, have demonstrated the material to be viable option for nanoreinforcement in cementitious composites. GNPs are formed by several layers of graphene, which is a single-layer sp^2-bonded carbon sheet, and are less prone to

agglomeration and entanglement because of their increased thickness [11]. Although the behavior of cementitious composites with CNTs and CNFs has been extensively studied by various researchers, limited work has been reported on the use GNPs in cementitious composites. Zohhadi et al. [12] investigated the use of surfactant-coated GNPs at two concentrations (0.05 and 0.5% by weight of the cement) in mortar cubes and cement paste beams. Results from compressive and flexural tests indicated that the well-dispersed GNPs can improve the flexural strength and stiffness of the cement paste. Wotring et al. [13] explored the effect of water reducing admixtures on GNP dispersion in water using scanning electron microscopy and ultraviolet-visible spectroscopy. Alkhateb et al. [14] studied the behavior of cement pastes with pristine and functionalized GNPs by correlating atomic assembly of the composite to its macroscopic behavior. Du and Pang [15] examined the barrier properties of GNP reinforced mortars and reported significant decrease in water penetration depth, chloride diffusion coefficient and chloride migration for the cement mortar with GNPs as compared to plain cement mortar. Tong et al. [16] investigated the effects of GNPs on the durability of cementitious composites and assessed the free-thaw performance and corrosion resistance of GNP-reinforced cement composites.

Pang et al. [17] and Le et al. [18] considered the addition of GNPs to ordinary cement mortars to enhance their electrical conductivity. The GNPs used in these studies had a diameter of 2.6 microns and a thickness of 2.6 nanometers, which yields an aspect ratio of 1000. The GNPs was mixed in water with a high range water reducer and ultrasonicated for 2 hours before adding the aqueous solution to the cement and sand mixture. The four-probe method was used to measure electrical resistivity of mortar specimens during compression and tension tests, and flexural tests on beam specimens with artificial notches were performed to assess damage sensing ability of the GNP reinforced mortars. The results of these studies indicated good strain-sensing and damage-sensing capabilities for the GNP reinforced mortars.

APPROACH

This study explores the development of self-sensing cementitious composites with GNPs using a simple fabrication method. For the detection of the percolation threshold, which roughly represents the optimal quantity of the GNPs required achieving satisfactory self-sensing, the specimens with following GNP concentration levels were prepared: 0%, 0.1%, 1%, 2.5%, 5%, and 7.5% by weight of cement using three different fabrication methods. The mixtures were cast into standard 40 mm × 40 mm × 160 mm prisms. Three specimens of each mixture were tested to ensure data reliability. For measuring the electrical resistivity, four copper mesh sheets were used as electrodes and embedded into the specimens immediately after casting. In addition, the use of copper tapes as electrodes and the use of a commercial resistivity meter for the resistivity measurements were explored. The electrical conductivity as a function of filler content of the GNP in the cementitious composites were plotted to determine percolation threshold. Cyclic compression tests were also conducted to explore the piezoresistive behavior of the specimens with different GNP concentrations.

METHODOLOGY

Materials

In order to determine the type of GNP that would be used in this study, an analytical prediction of the percolation threshold was employed. Li and Kim [19] suggested the following equation to predict the percolation threshold of conducting polymer composites containing disc-shaped nanoparticles with high aspect ratios:

$$V_f = \frac{27\pi D^2 t}{4(D + D_{IP})} \quad (1)$$

where V_f is the critical volume fraction of ratio 3D nanoplatelets, D is the diameter of GNP, t is the thickness of GNP, and D_{IP} is the interparticle distance. The D_{IP} is expected to be on the order of 10 nm, while the smallest diameter of the commercially available GNPs considered in this study and provided by XG Sciences was about 2×10^3 nm. Therefore, the above equation can be simplified as:

$$V_f = \frac{27\pi}{4}\left(\frac{t}{D}\right) \quad (2)$$

The results of percolation threshold calculations for different types of GNPs are shown in the Table 1. It can be seen that Grade M GNPs with a diameter of 25 µm has the lowest percolation threshold that is predicted by the equation (2), and thus was chosen for the experimental studies. Note that the effects of GNP characteristics such as aspect ratio and surface area on the conductivity of cementitious composites needs to be more thoroughly investigated, but it is out of scope of the current study. The properties of Grade M-25 GNPs are shown in Table 2 below.

Table 1. Calculations of Percolation Thresholds for Different Types of GNPs

GNP Type	Diameter (µm)	Thickness (nm)	Surface Area (m^2/g)	V_f (%)
H-5	5	15	50~80	6.4
H-15	15	15	50~80	2.1
H-25	25	15	50~80	1.3
M-5	5	6~8	120~150	3.4
M-15	15	6~8	120~150	1.1
M-25	25	6~8	120~150	0.7
C-300	<2	1~2	300	2.1
C-500	<2	1~2	500	2.1
C-750	<2	1~2	750	2.1

Portland cement type I/II and ASTM C778 graded sand were used in the mortar mixture. A superplasticizer, AdvaCast 575, was used to disperse the GNPs into the mixing water and to increase the workability of the GNP reinforced mortar.

Table 2. Properties of GNP M-25

Properties	**Values**
Surface Area (m^2/g)	120~150
Diameter (μm)	25
Thickness (nm)	6-8
Density (g/cc)	2.2
Carbon Content (%)	>99.5
Tensile Modulus (GPa)	1000
Tensile Strength (GPa)	5

Mixing Procedures

Three different methods were considered in this study to fabricate GNP reinforced mortar specimens considering the findings of the study conducted by Al-Dahawi et al [20]. The three mixing procedures are summarized and illustrated in Figure 1.

In Method I, the GNP was measured and added to the total amount of mixing water and superplasticizer (AdvaCast 575). The beaker containing the solution was placed in a bath ultrasonicator for 1.5 hours. Before ultrasonication was completed, the cement and sand were mixed in a Hobart commercial mixer for 10 min at 125 rpm. Following this, the GNP solution was removed from the ultrasonicator and added to the dry materials over a period of 10 seconds. The mixing speed was increased to 300 rpm and the materials were mixed for an additional 10 min and then cast into molds.

In Method II, the dry materials including the GNP, sand and cement were first mixed in a Hobart commercial mixer for 10 min at 125 rpm. The mixing water was then added to the dry materials over 10 s. The mixer speed was increased to 300 rpm and the superplasticizer (AdvaCast 575) was added into mixer over 30 seconds.

In Method III, the GNP and superplasticizer (AdvaCast 575) were measured out and added to the mixing water. A kitchen-type blender was used to mix the GNP suspension at 3000 rpm for 15 min. During this time, the cement and sand were mixed in a Hobart commercial mixer at 125 rpm for 10 min. The GNP suspension was then added to the mixer over 10 seconds and mixing continued for an additional 10 min at 300 rpm. The mortar was then cast into the molds. Note that the last two methods do not require any special treatment techniques.

Method 1:

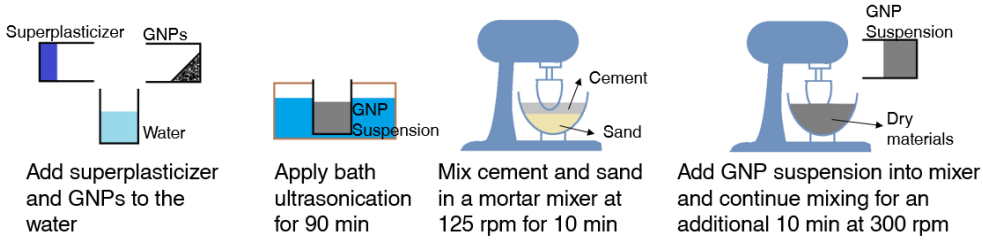

Add superplasticizer and GNPs to the water | Apply bath ultrasonication for 90 min | Mix cement and sand in a mortar mixer at 125 rpm for 10 min | Add GNP suspension into mixer and continue mixing for an additional 10 min at 300 rpm

Method 2:

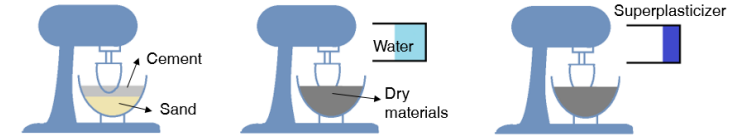

Mix cement, sand and GNPs in a mortar mixer at 125 rpm for 10 min | Add water into mixer over 10 s | Add superplasticizer into mixer over 30 s and continue mixing for an additional 10 min at 300 rpm

Method 3:

Add superplasticizer and GNPs to the water | Mix the suspension with a hand-held mixer at 3000 rpm for 15 min | Mix cement and sand in a mortar mixer at 125 rpm for 10 min | Add GNP suspension into mixer and continue mixing for an additional 10 min at 300 rpm

Figure 1. Fabrication procedures

Sample Preparation

Seven separate batches of mortar containing various levels of graphene nanoplatelets were prepared using the three mixing methods described above. Each batch of mortar was prepared as per ASTM C109, maintaining a water to cement ratio of 0.485. Type I/II cement, water and natural silica sand were used in the mix design. Standard prismatic mortar specimens of dimensions 40 mm × 40 mm × 160 mm containing GNPs at six different concentrations (0%, 0.1%, 1%, 2.5%, 5%, and 7.5% by weight of the cement) were prepared.

The amount of superplasticizer was chosen to be 50% by mass of GNPs based on recommendations from the study by Du and Pang [15]. However, when trial batches of mortars with 5% and 7.5% GNP were prepared, the amount of superplasticizer was not sufficient to obtain good workability of the mixture. Note that the Grade M-25 GNPs have a surface area that is about 380 times larger than Portland cement, which indicates the need for higher amounts of superplasticizer. Therefore, the amount of superplasticizer for the mortars with 5% and 7.5% GNP batches was recalculated to take into account the higher surface area of GNPs, and the dosage of superplasticizer for 5% and 7.5% was increased to 40 ml (41.20 g) and 60 ml (62.30 g). Table 3 summarizes the mix proportions for each batch of mortars

Table 3. Mixture Proportions

Batch	GNP (wt% of cement)	GNP (g)	Superplasticizer (g)	Cement (g)	Water (g)	Sand (g)
1	--	--	--	583.0	335.7	1603.3
2	0.1	0.58	0.29	583.0	335.7	1603.3
3	1	5.83	2.92	583.0	335.7	1603.3
4	2.5	14.58	7.29	583.0	335.7	1603.3
5	5	29.15	41.20	583.0	335.7	1603.3
6	7.5	43.73	62.30	583.0	335.7	1603.3
7	2.5	14.58	7.29	583.0	335.7	1603.3

One other batch with 2.5% GNP ratio was also prepared to assess the effect of electrode type used for the measurements. Three specimens were prepared for each batch.

In addition, another seven batches of mortar containing graphene nanoplatelets and Class F fly ash were prepared using mixing method III. In these batches, 20% of cement was replaced by fly ash, while the other ingredients remained the same. The proportions for these bathes were shown in Table 4.

Table 4. Mixture Proportions for Mortar with Fly Ash

Batch	GNP (wt% of cement)	GNP (g)	Superplasticizer (g)	Fly ash (g)	Cement (g)	Water (g)	Sand (g)
1	--	--	--	116.6	466.4	335.7	1603.3
2	0.1	0.58	0.29	116.6	466.4	335.7	1603.3
3	1	5.83	2.92		466.4	335.7	1603.3
4	2.5	14.58	7.29		466.4	335.7	1603.3
5	5	29.15	41.20		466.4	335.7	1603.3
6	7.5	43.73	62.30		466.4	335.7	1603.3
7	2.5	14.58	7.29		466.4	335.7	1603.3

Four copper mesh sheets were embedded into each specimen to serve as electrodes. One additional batch with 2.5% GNPs was prepared to make the measurements with copper tape and silver paint that were used as electrodes (Figure 2a). The spacing between the outer probes were set as 120 mm and the spacing between the inner probes were set as 80 mm.

Measurements

Electrical resistivity measurements were conducted using the four-probe method. The resistance of the mortar specimen, *R*, was calculated using the equation:

$$R = \frac{V}{I} \tag{3}$$

where *V* is the applied voltage and *I* is the current through specimens.

The resistivity of GNP reinforced mortar specimens was calculated using the equation shown below:

$$\rho = \frac{RS}{L} \tag{4}$$

where *S* is the area of the cross section and *L* is the distance between two inner probes.

To measure the electrical resistance two digital multimeters were used. A GW INSTEK programmable power supply was used to supply direct current (DC) up to 20 V. One of the multimeters, which was connected to the outer probe and power supply, was used to measure the current intensity, and the other multimeter, which was connected to the inner probe, was used for voltage difference measurement.

A concrete resistivity meter manufactured by Proceq was also used to measure the surface resistivity of the specimens. The four probes of the device were equally spaced at 50 mm and two other probes applied a steady current while two inner probes measured the current difference as shown Figure 2(b).

A 22 kips MTS loading machine was used to do the cyclic compression test. The electrical resistance was recorded during the testing as shown Figure 2(c). Here, the response of the specimens cast using Method I is discussed for the cyclic loading. The amplitude of load for the specimens with 7.5% GNPs was 3 kN, while the amplitude of the rest specimens was 10 kN. For each specimen, the loading rate was 0.05 kN/s and the tests were conducted for 3 cycles.

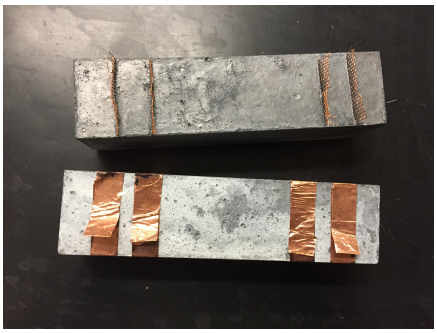

(a)

(b)

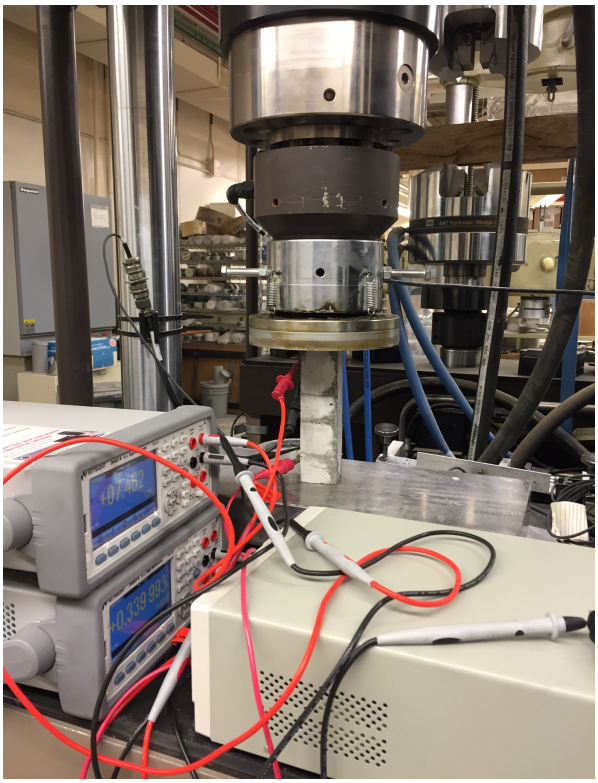

(c)

Figure 2. (a) Specimen with copper tape and meshes; (b) Resistivity meter measurement; (c) Cyclic compression test measurement.

FINDINGS

Electrical Resistivity

The electrical resistivity measurements were made at 1 day, 7 days, 14 days, and 28 days for the specimens cast using the three different methods. Figures 3 to 6 show the average resistivity as well as the standard deviation of the specimens prepared with different mixing methods. It can be see that, for most of the specimens, the resistivity increased with an increase in curing age. The increase in the resistivity values can be attributed to the change in the mortar microstructure resulting from cement hydration that leads finer pores. However, the rate of the increase was reduced with the extended curing. For example, although there was a clear difference between 1-day and 7-day measurements for the specimens cast using Method I, the resistivity measurements at 14-day and 28-day were quite similar for the same specimens.

Figure 7 shows the average values of resistivity of the specimens with different amount of GNPs at different curing ages. It can be seen that the variation of average resistivity with different GNP ratios follows a similar trend for three mixing methods at each curing age. For different curing ages, there is a sharp decrease in the electrical resistivity when the GNP ratio was over 5%. The addition of GNPs less than 5% by weight of cement did not improve the

electrical conductivity as compared to the plain mortar as the amount of GNPs was not likely enough to form a conductive network. Actually, for three mixing methods, the resistivity of specimens with 2.5% GNPs was considerably higher than the plain mortar specimens. This can be attributed to the agglomerates occurred in the matrix due to the poor dispersion of GNPs. The largest decrease in the resistivity was observed for 7.5% GNP ratio. Therefore, the amount of GNPs might exceed the percolation threshold for that GNP concentration.

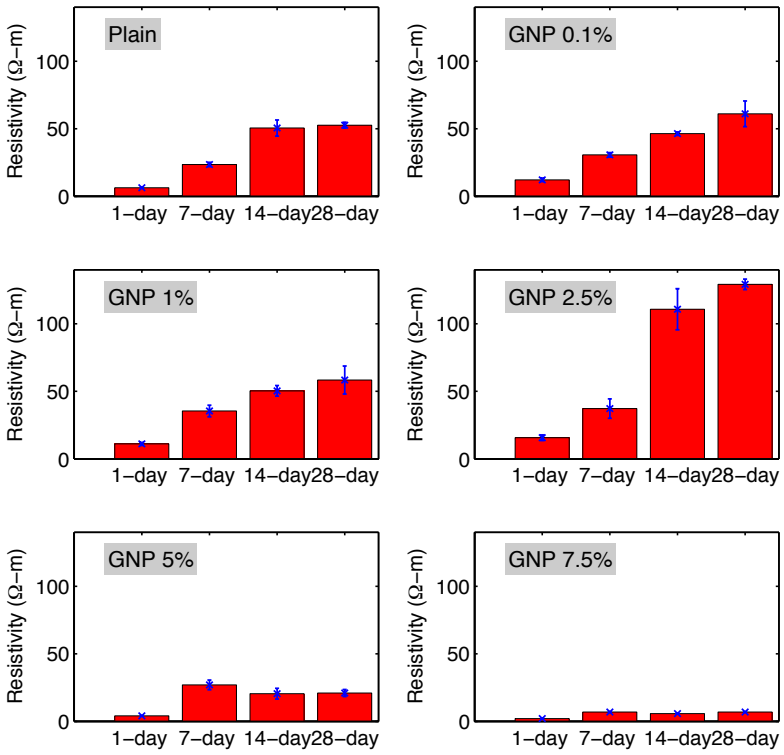

Figure 3. Average resistivity of specimens cast using Method I.

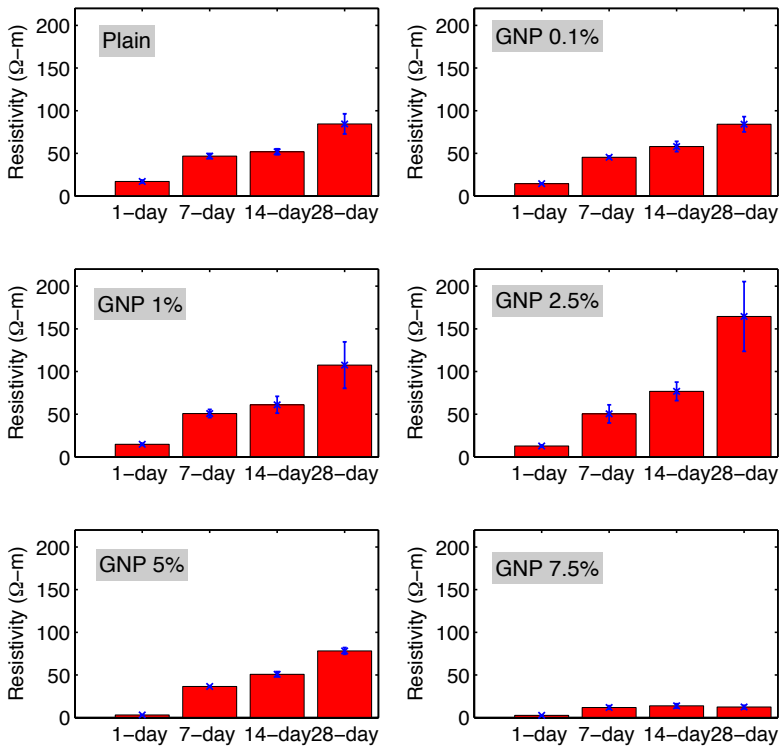

Figure 4. Average resistivity of specimens cast using Method II.

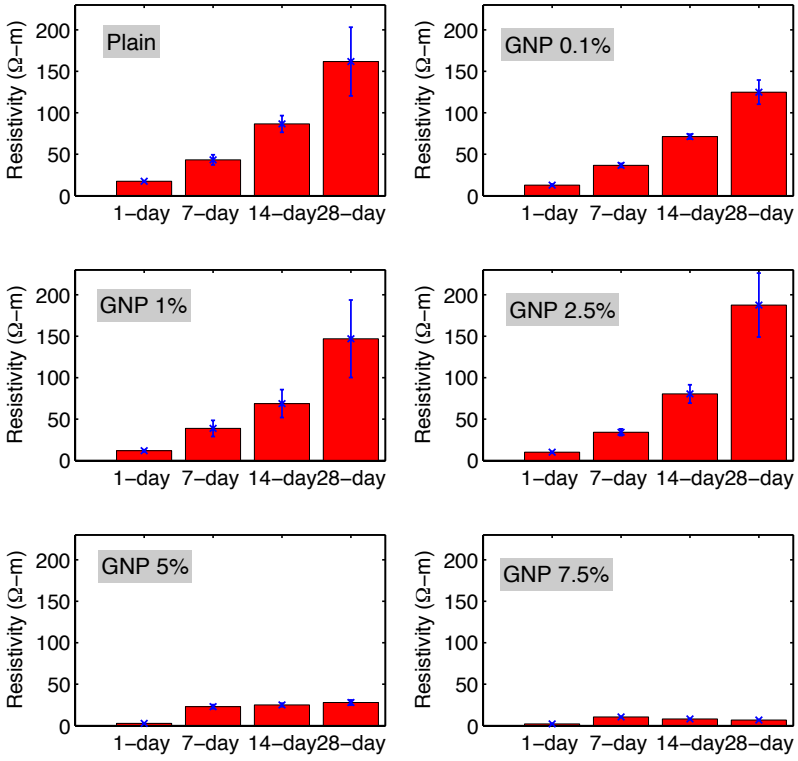

Figure 5. Average resistivity of specimens cast using Method III.

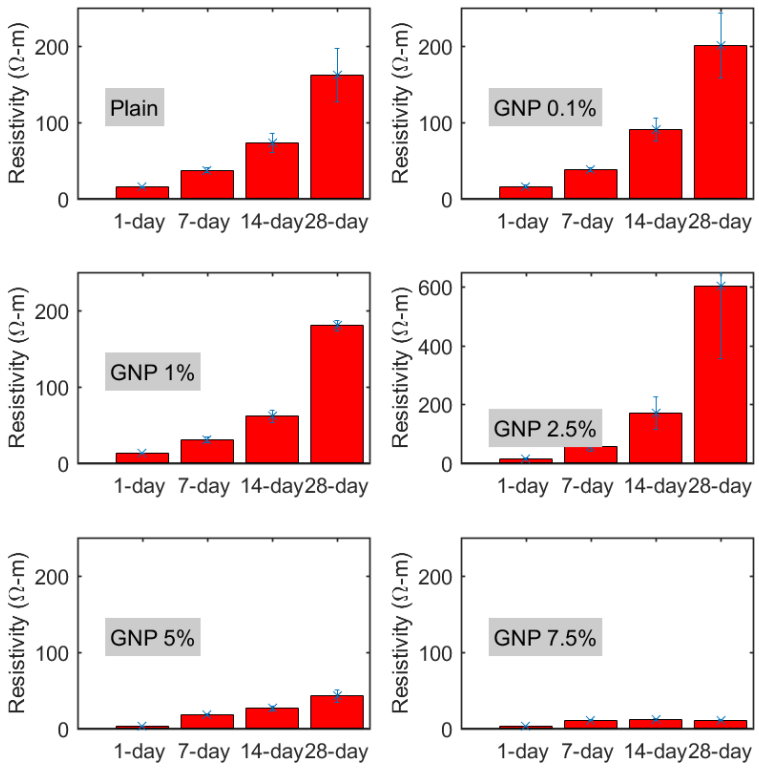

Figure 6. Average resistivity of specimens with fly ash

Note that for the specimens with 2.5, 5% and 7.5% GNPs by weight of cement, the corresponding volume fraction of GNPs in the mortar mixture are 0.6%, 1.1% and 1.5%. The analytical prediction of 0.7% by volume of mixture suggests a lower bound as the actual GNP particles are not uniform. The experimental results indicate that the critical volume ratio should be over 1%.

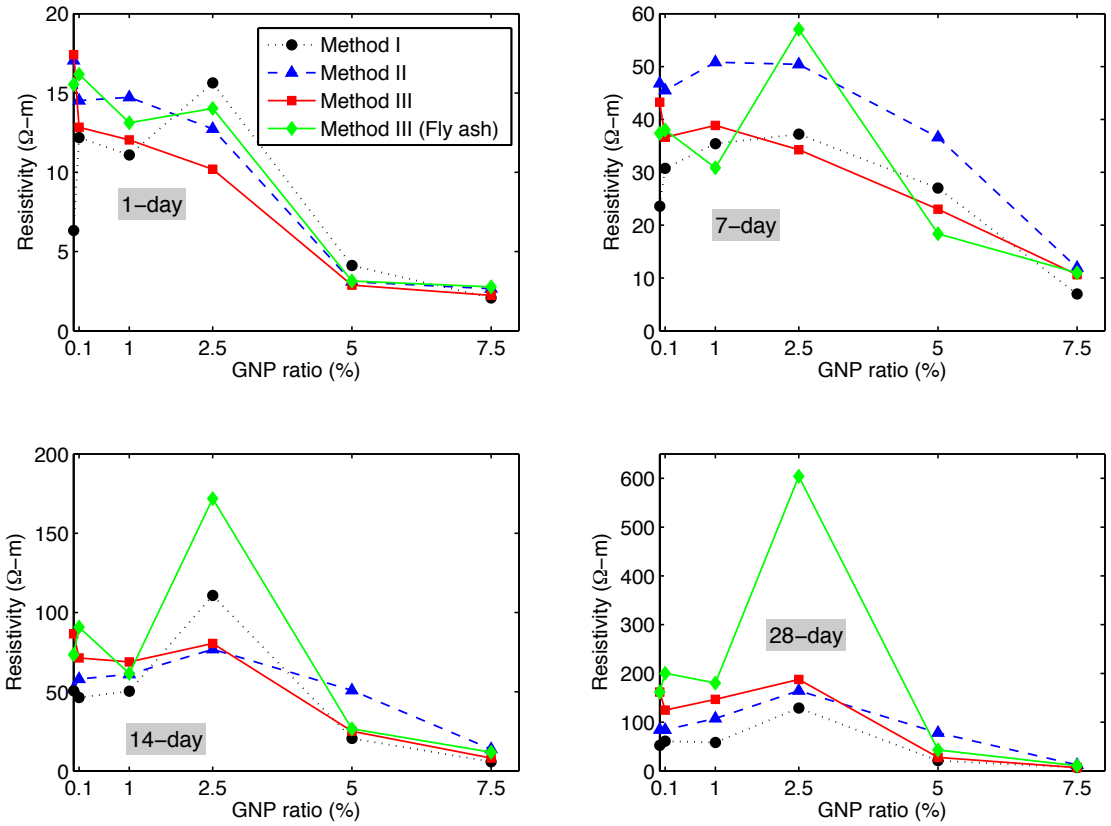

Figure 7. Electrical resistivity of different specimens at (a) 1 day; (b) 7 days; (c) 14 days; (d) 28 days.

The electrical resistivity measurements obtained using different measurement methods are listed in Table 5. A resistivity meter and embedded copper meshes were used to measure the resistivity of specimens in the 4th batch, while the resistivity meter and copper tapes were used for the measurements in the 7th batch. As shown in the Table 5, the resistivity values measured by the resistivity meter were much higher than those measured with the copper tapes and the embedded copper meshes. For the specimens cast using Method I, using the ratio of the resistivity measurements obtained with resistivity meter in the 4th and 7th batches, the resistivity of the 7th batch can be calculated to be 86.4 Ω-m if the copper meshes were used to measure the resistivity. This value is very close to the resistivity measured using copper tape for the 7th batch, which suggest that measurements with the copper tape and copper mesh produce similar results. Similar observations were made for the specimens cast using Method II and III. Although the resistivity measured with the resistivity meter had higher values as compared to those made with embedded meshes, a similar trend of change with different GNP ratios were observed for both measurement methods as shown in Figure 8.

Table 5. Resistivity Measurements with Different Methods at 28 Days

Mixing Method	Batch	Measurement	Average Resistivity, ρ (Ω-m)
Method I	4	Resistivity meter	670.2
	4	Copper meshes	129.2
	7	Resistivity meter	448.3
	7	Copper tape	85.1
Method II	4	Resistivity meter	685.8
	4	Copper meshes	164.5
	7	Resistivity meter	428.4
	7	Copper tape	90.0
Method III	4	Resistivity meter	747.3
	4	Copper meshes	187.55
	7	Resistivity meter	901.7
	7	Copper tape	246.3

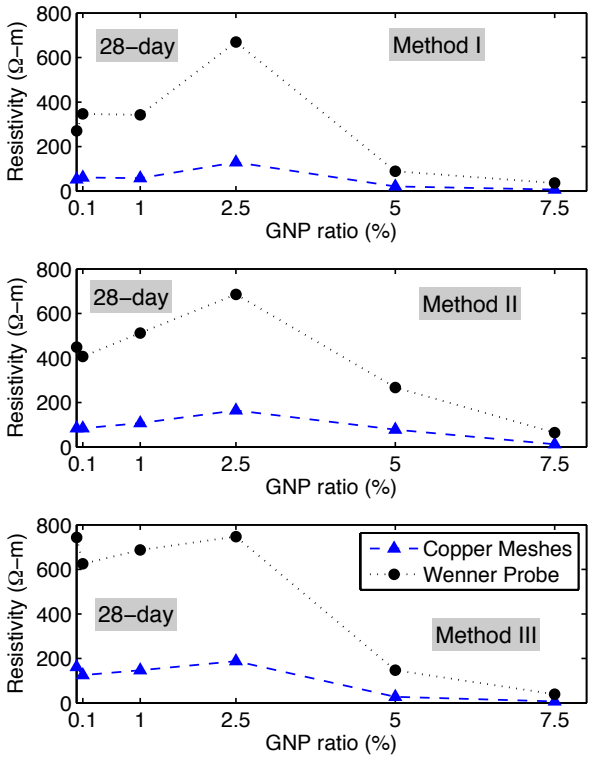

Figure 8. Comparison of results measured using Wenner probe and copper meshes.

Cyclic Compression Test

The strain sensing capacity of a material can be described as the response on the volumetric electrical resistivity due to its strain state. When under compression, the electric

resistance in that direction undergoes a decreasing trend. On the other hand, the electrical resistance increases when the material is under tension as the fillers trends to separate. Since the both effects are reversible in the elastic range of the material, the electrical resistance returns its initial value upon unloading [4].

Figures 9 and 14 display the cyclic compression response to the specimens cast using Method I. The fractional change in resistivity was calculated using the following equation:

$$\mathrm{FCR} = \frac{\rho_t - \rho_0}{\rho_0} \qquad (5)$$

where ρ_t is the resistivity at time t during the compression test; and ρ_0 is the resistivity measured prior to loading.

It can be seen from Figures 9 to 11 that there is no clear relation between the applied load and the change in resistivity for all specimens with 0%, 0.1%, and 1% GNPs. For one of the specimens with 2.5% GNPs, there is a decrease in the resistivity with an increase of compression load and an increase in the resistivity when the load is removed. However, the behavior is highly nonlinear. Also, the other two specimens with 2.5% GNPs did not show this phenomenon. For these two specimens, the resistivity value constantly increased with an increase in loading (Figure 12), which might be due to the tiny cracks that appeared inside of the specimens.

On the other hand, for the specimens with 5% and 7.5% GNPs, the resistivity values decreased with an increase in compression load, while the resistivity increased during the unloading during each loading cycle (Figures 13 and 14). For one of the specimen with 5% GNPs, that behavior was not clearly exhibited in the first loading cycle. Also, the response was more nonlinear for the specimens with 5% GNPs compared to those of the specimens with 7.5% GNPs. In particular, the rate of decrease in resistivity reduced with increasing load.

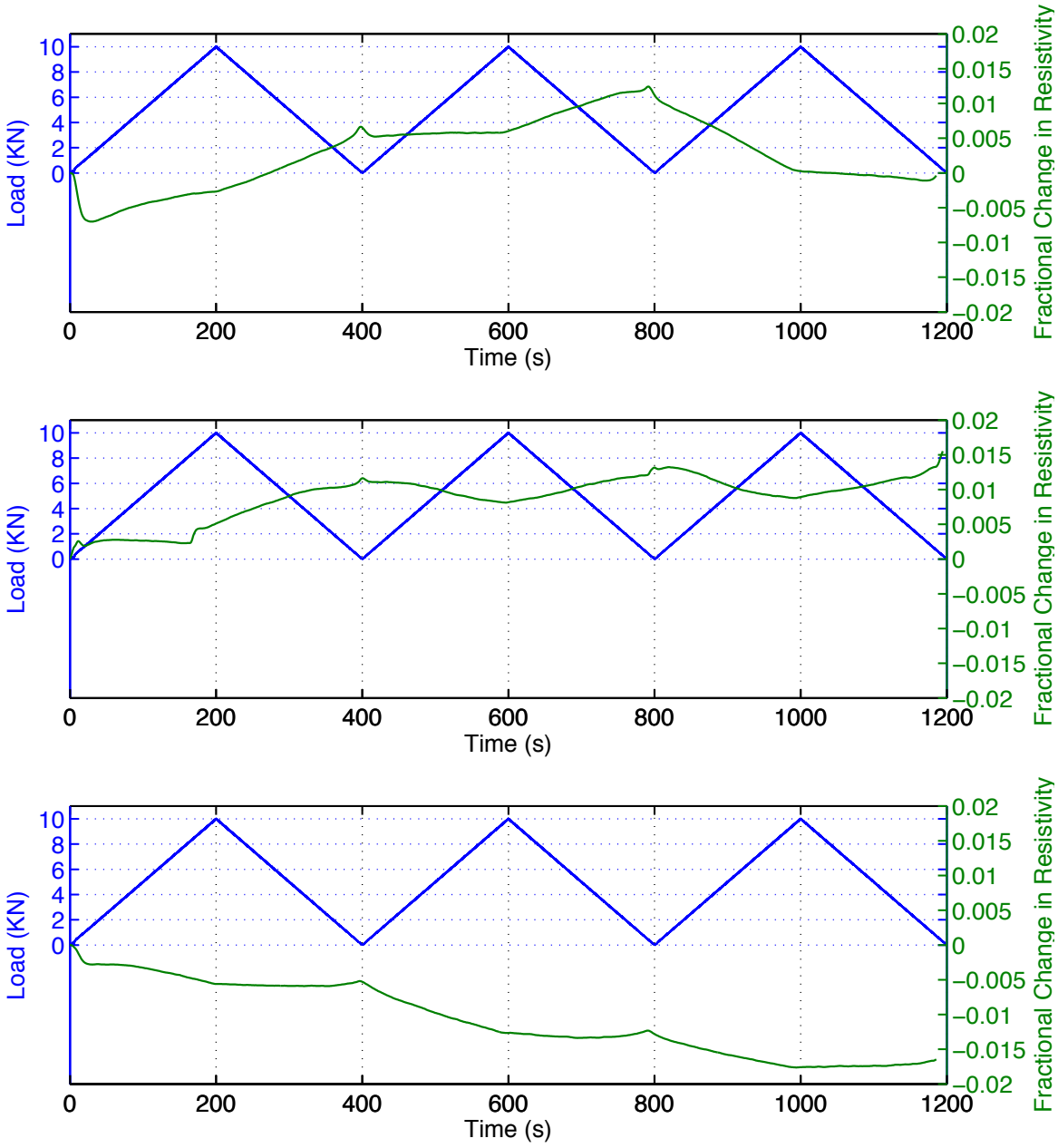

Figure 9. Cyclic compression response of specimens with 0% GNPs casted using Method I

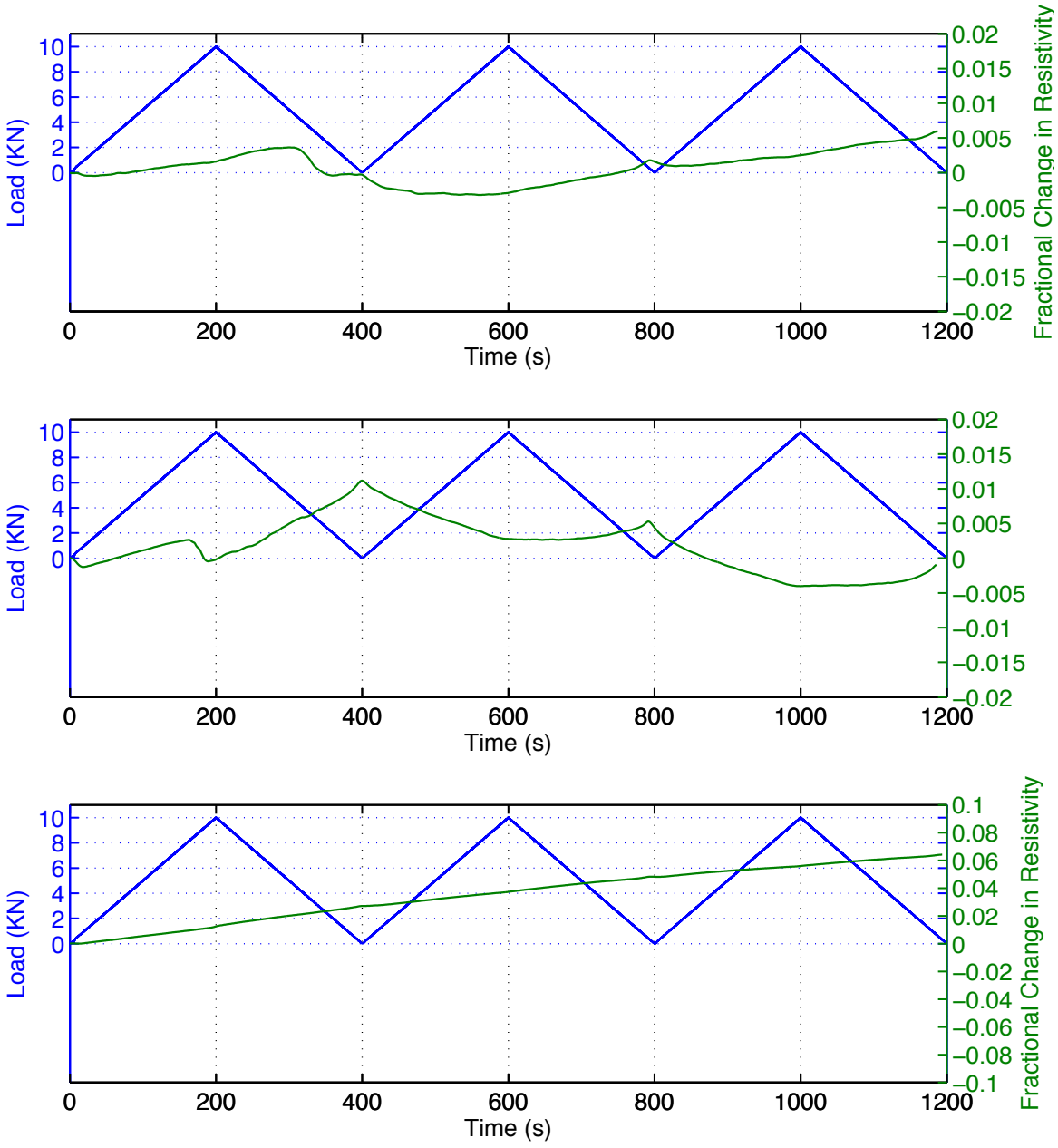

Figure 10. Cyclic compression response of specimens with 0.1% GNPs casted using Method I

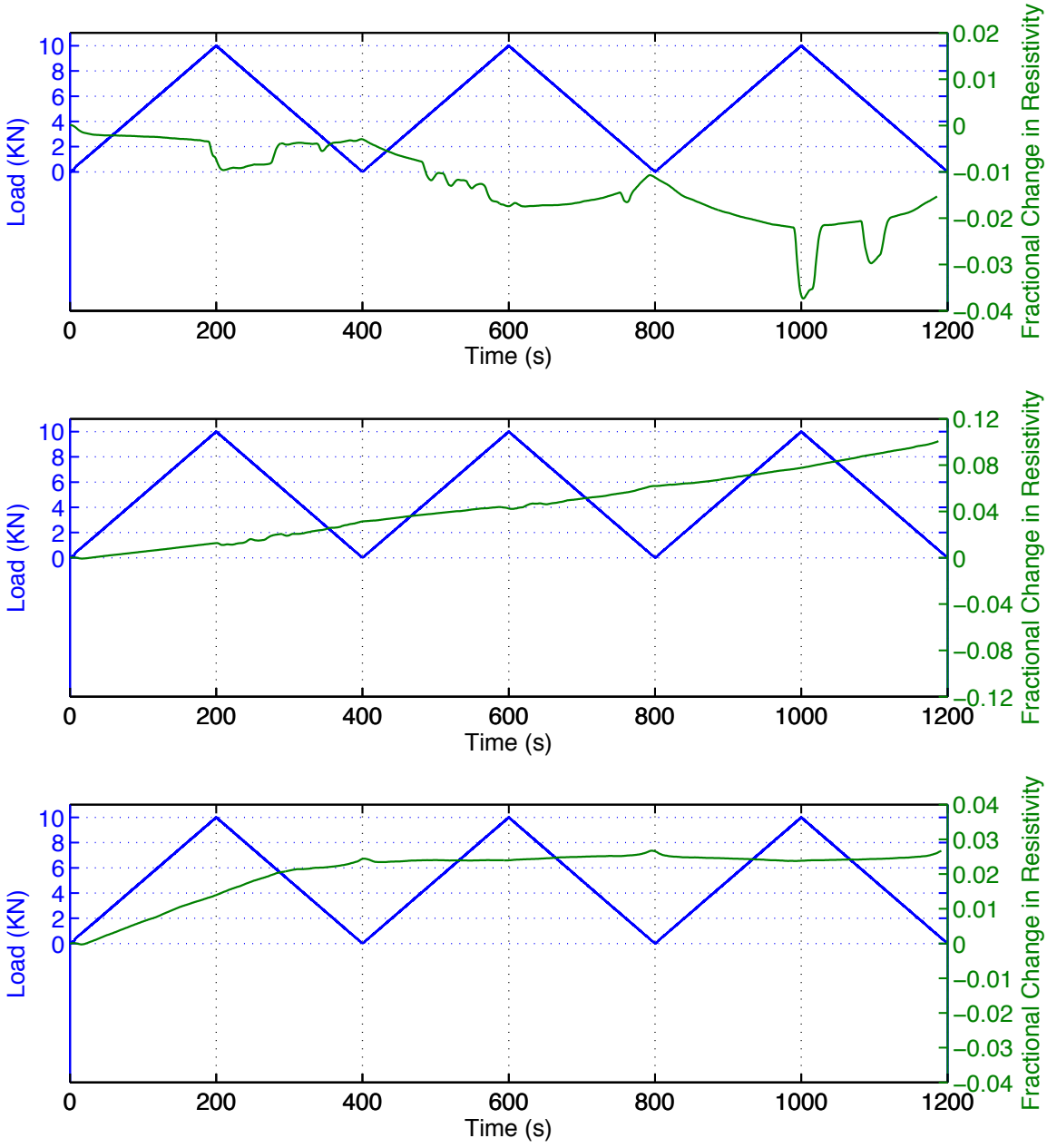

Figure 11. Cyclic compression response of specimens with 1% GNPs casted using Method I.

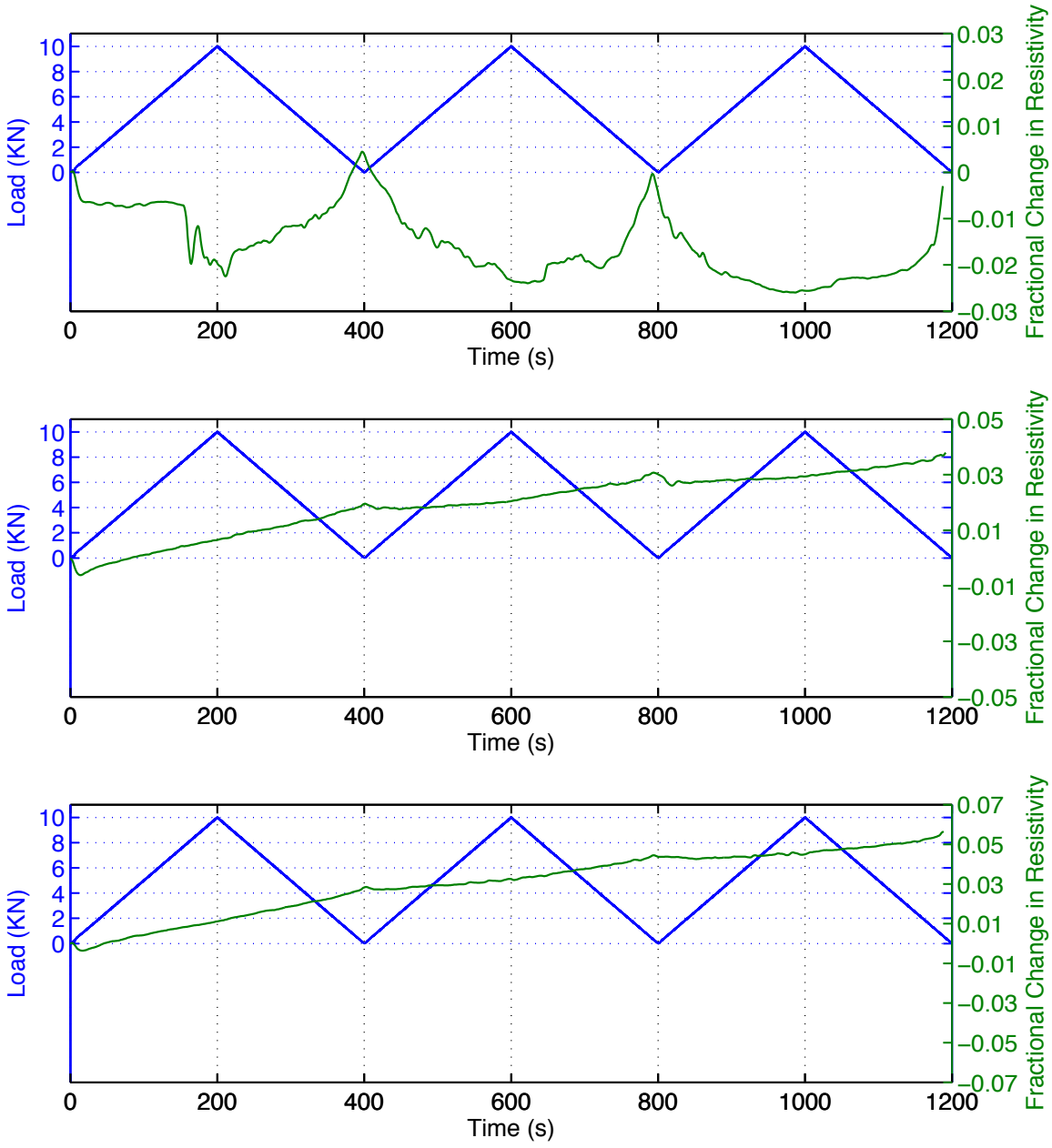

Figure 12. Cyclic compression response of specimens with 2.5% GNPs casted using Method I.

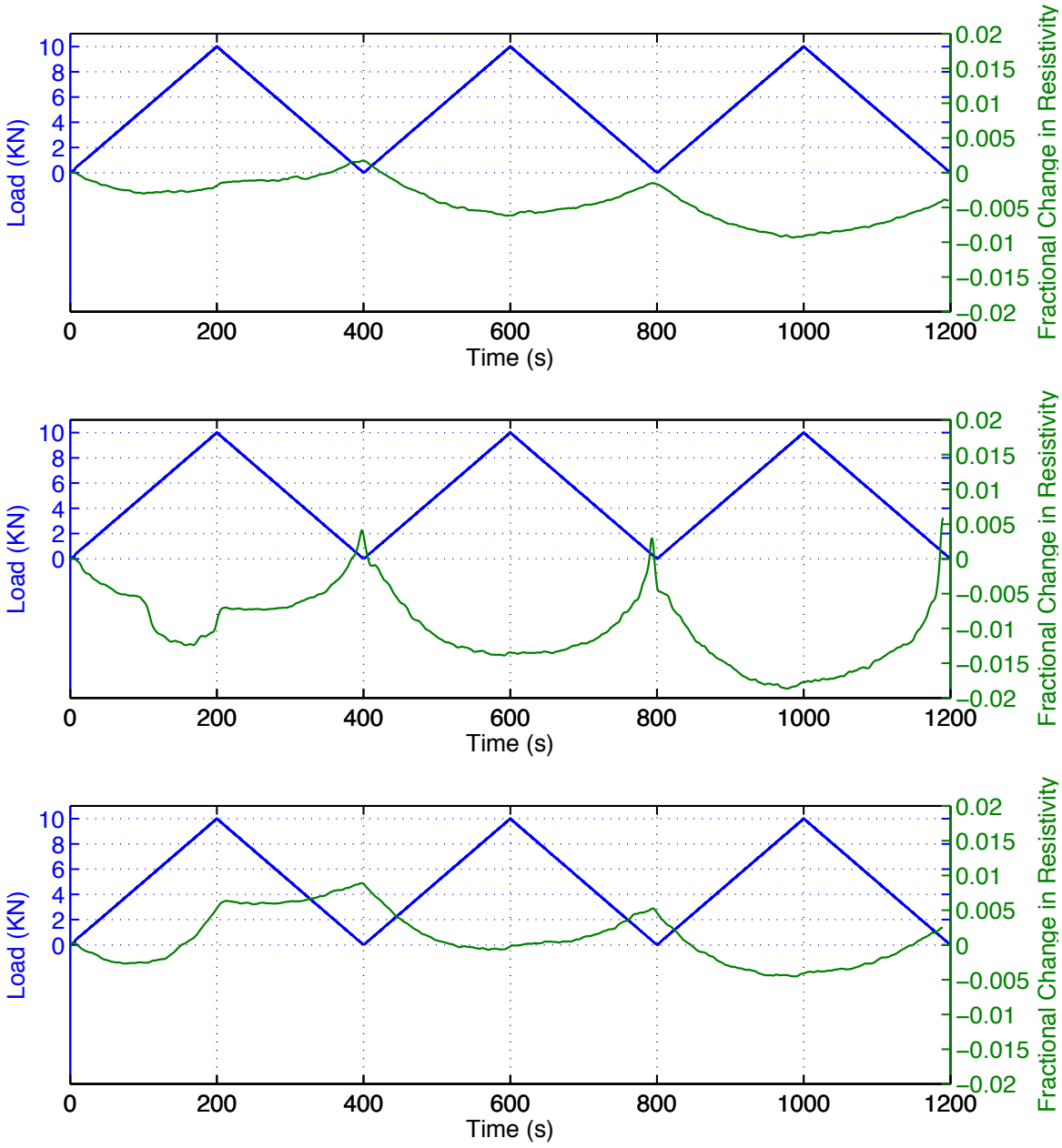

Figure 13. Cyclic compression response of specimens with 5% GNPs casted using Method I.

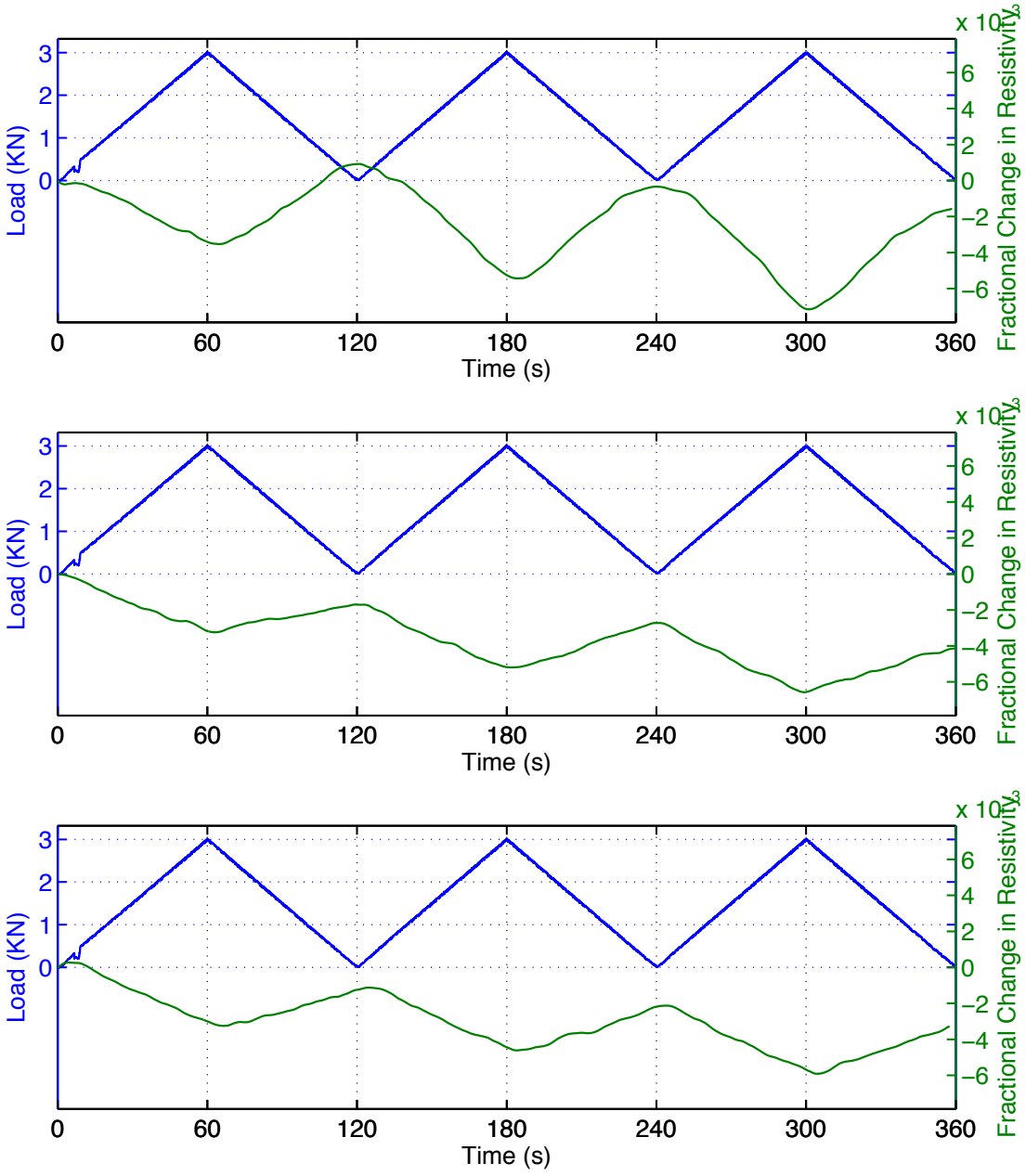

Figure 14. Cyclic compression response of specimens with 7.5% GNPs casted using Method I.

Figures 15 and 20 display the cyclic compression response to the specimens cast using Method II. It can be seen from Figure 9 that there is no clear relation between the applied load and the change in resistivity for all specimens with 0%, 0.1%, 1% and 2.5 GNPs.

Similar to the specimens casted using Method I, for the specimens with 5% and 7.5% GNPs (Figures 19 and 20), the resistivity values decreased with an increase in compression load, while the resistivity increased during the unloading during each loading cycle. The specimens with 5% GNPs casted with Method II exhibited better piezoresistive behavior compared to the behavior of the specimens with 5% GNPs casted with Method I.

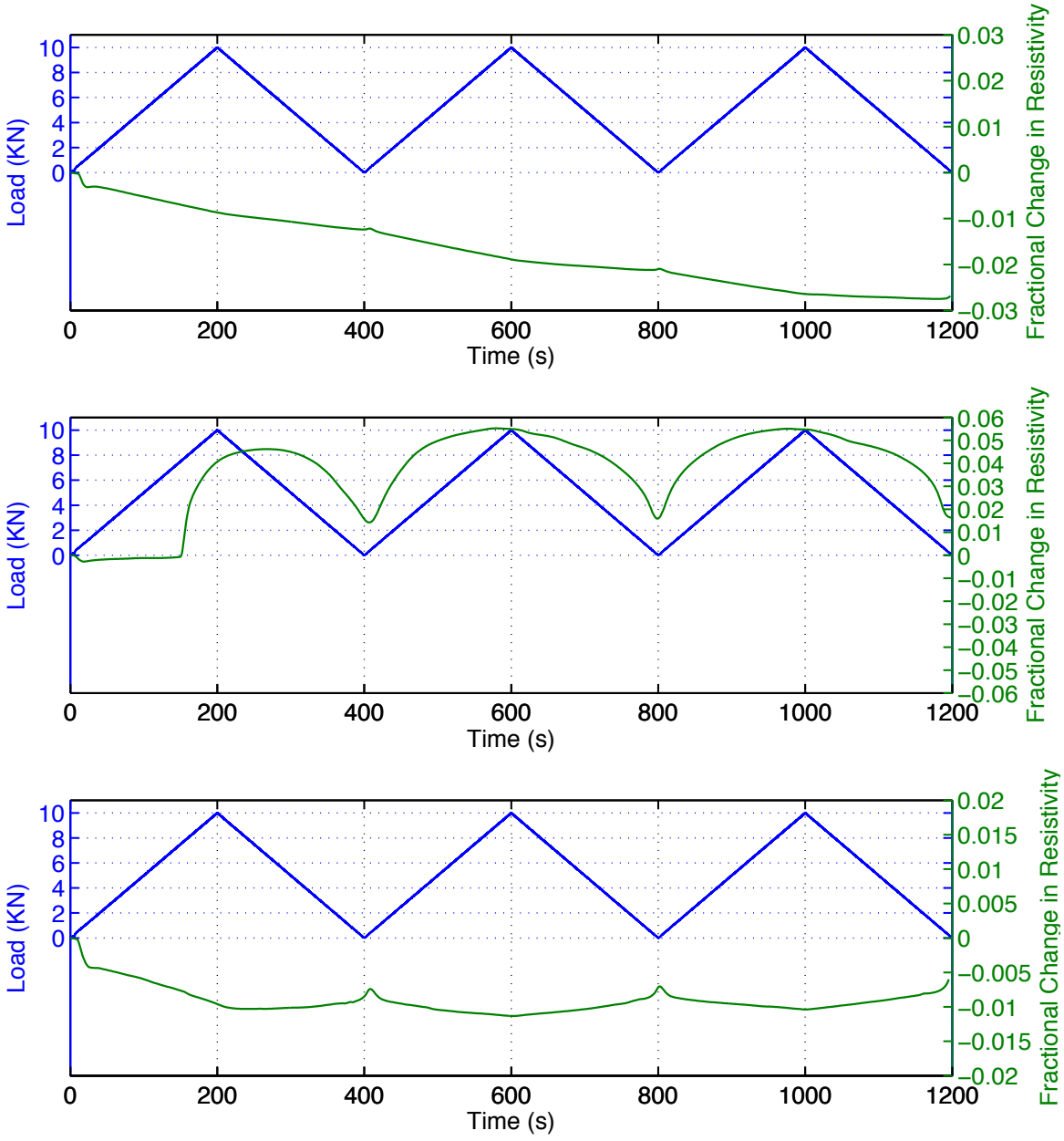

Figure 15. Cyclic compression response of specimens with 0% GNPs casted using Method II

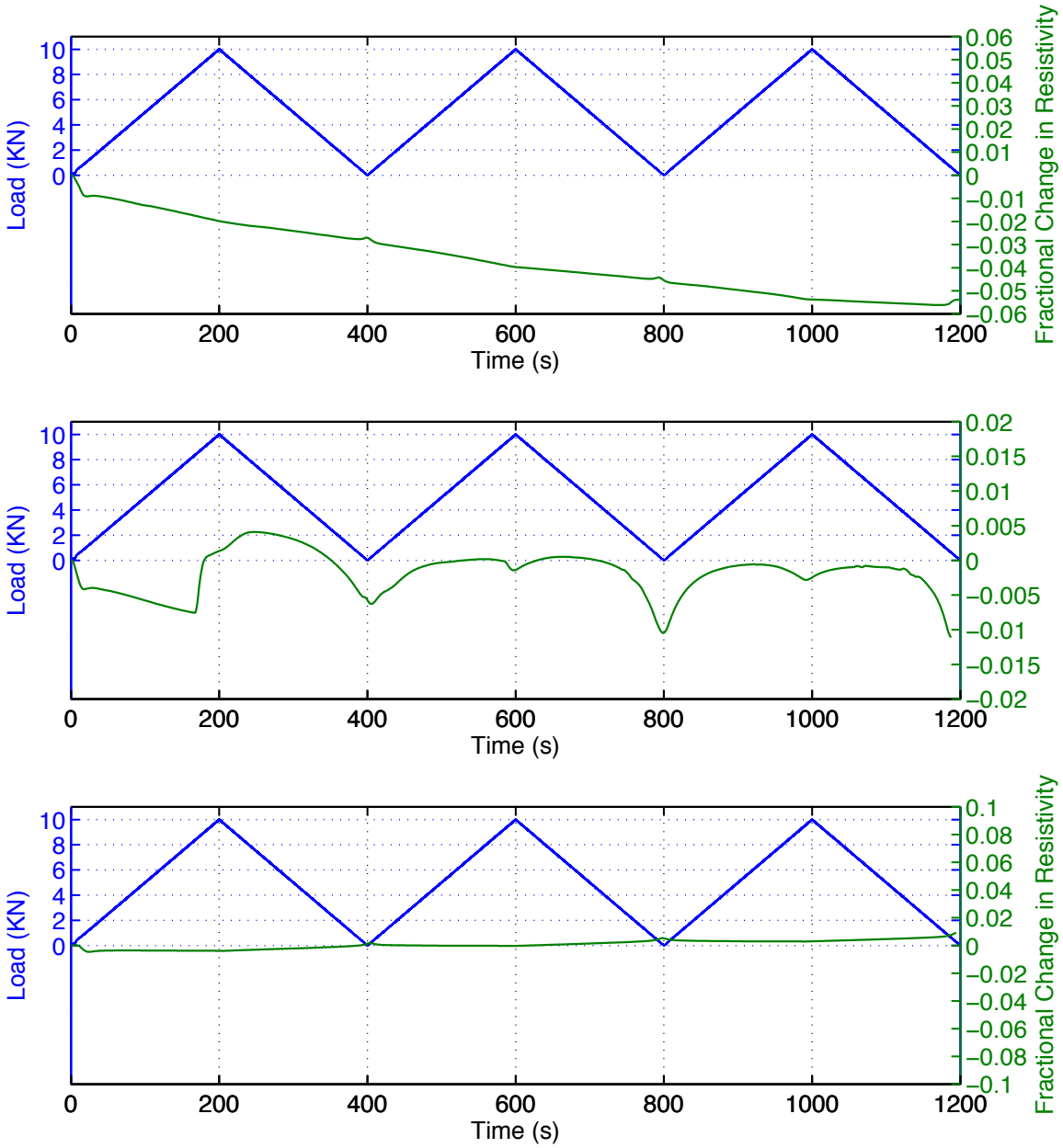

Figure 16. Cyclic compression response of specimens with 0.1% GNPs casted using Method II

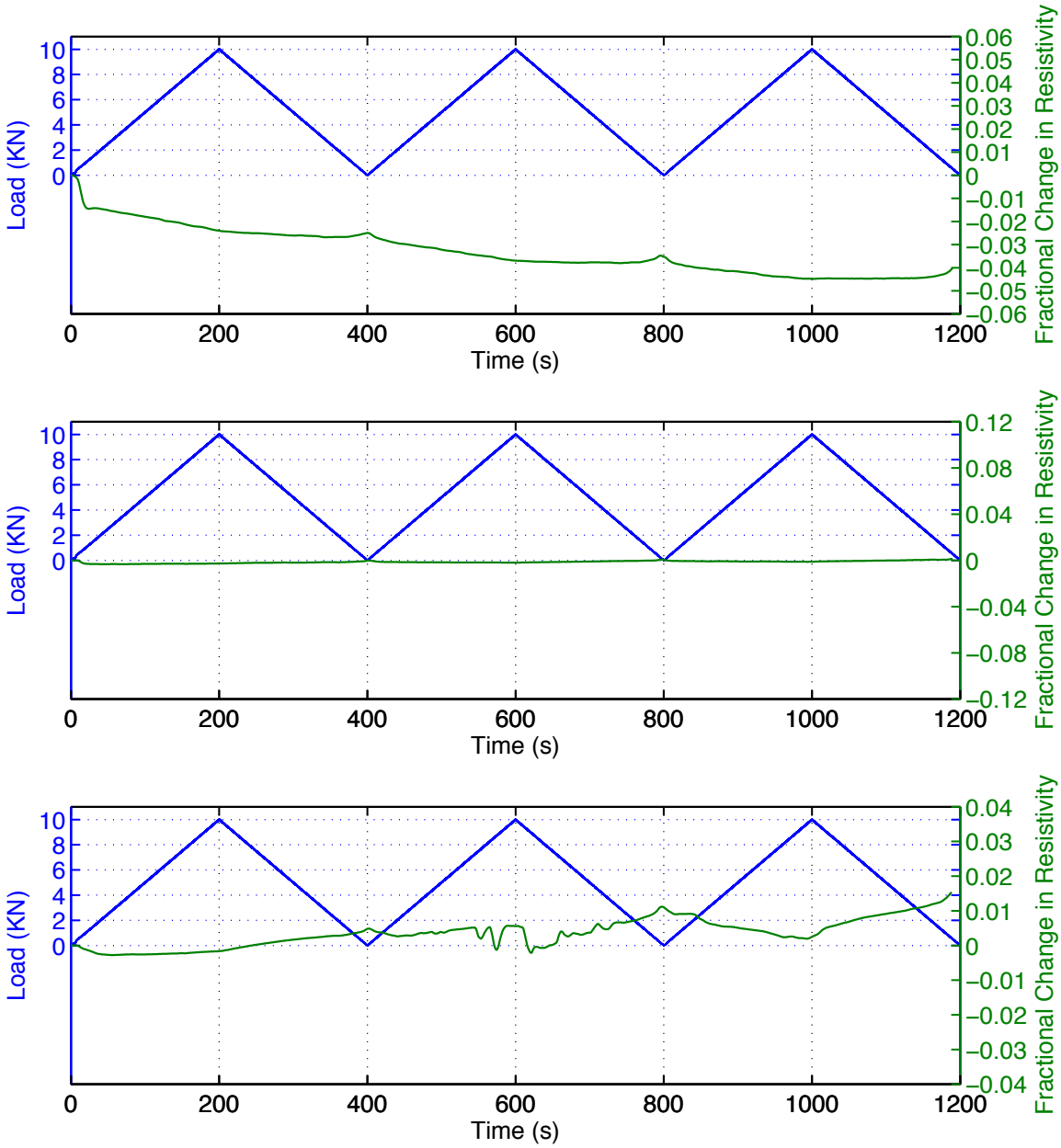

Figure 17. Cyclic compression response of specimens with 1% GNPs casted using Method II

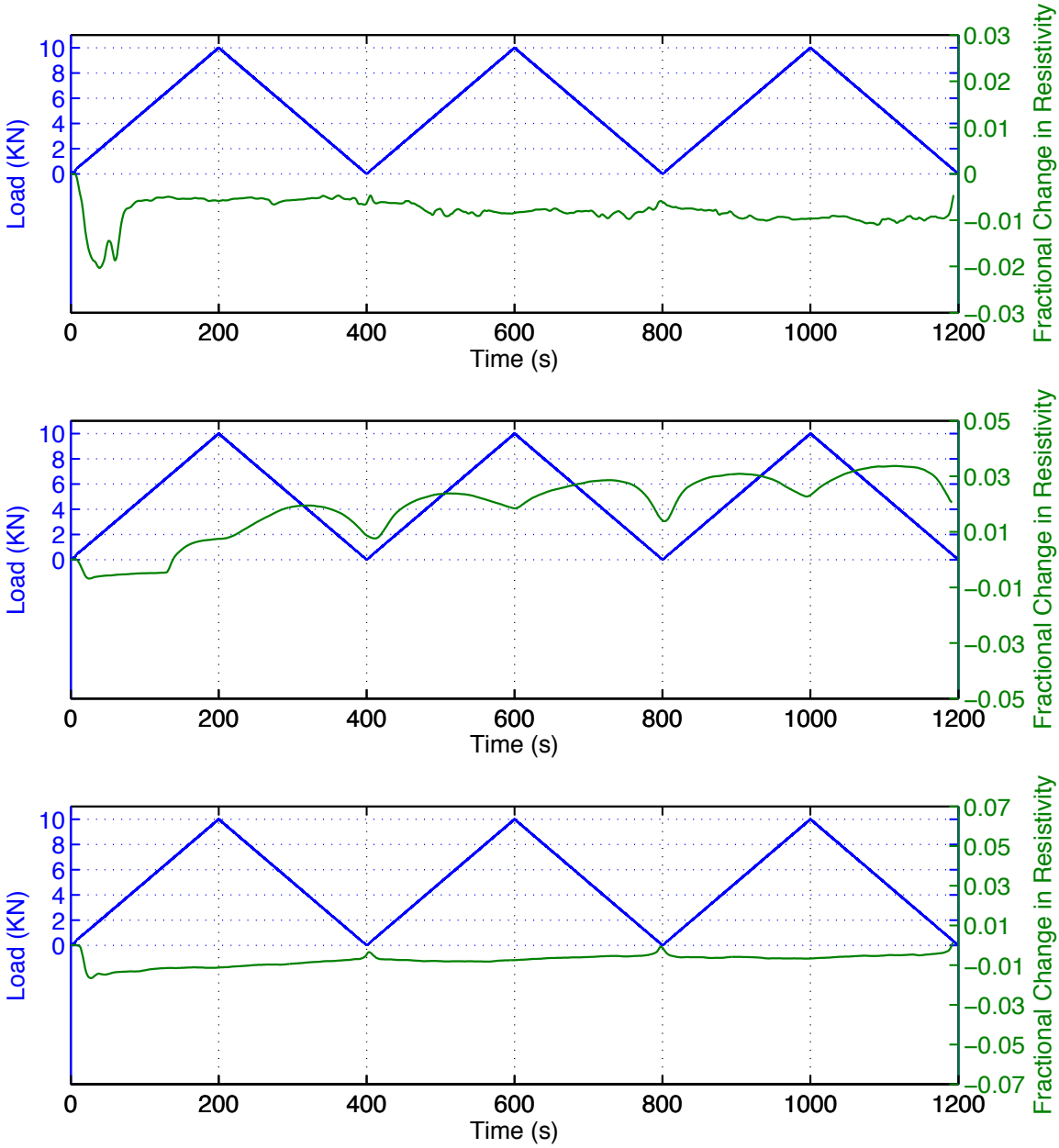

Figure 18. Cyclic compression response of specimens with 2.5% GNPs casted using Method II

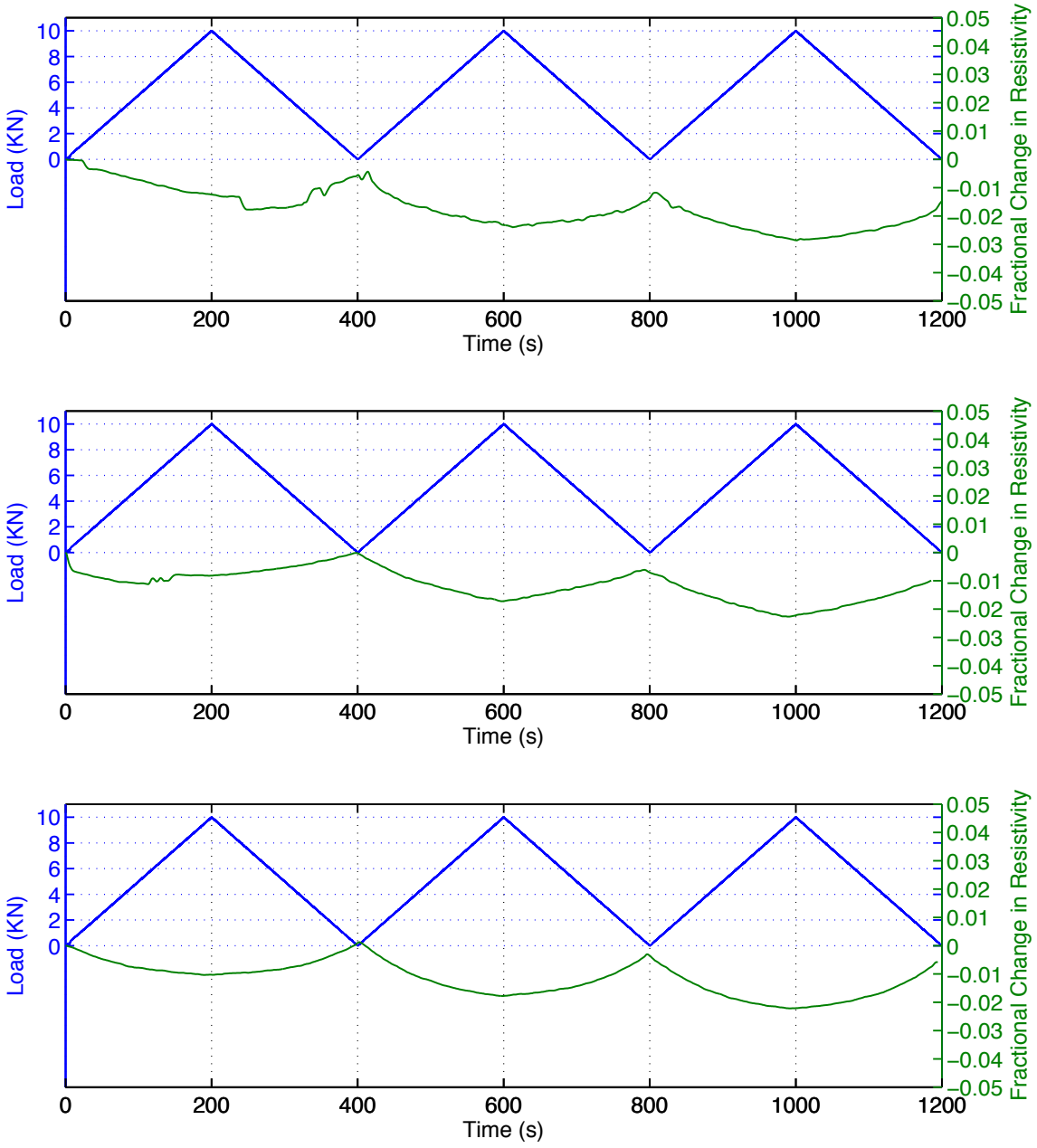

Figure 19. Cyclic compression response of specimens with 5% GNPs casted using Method II

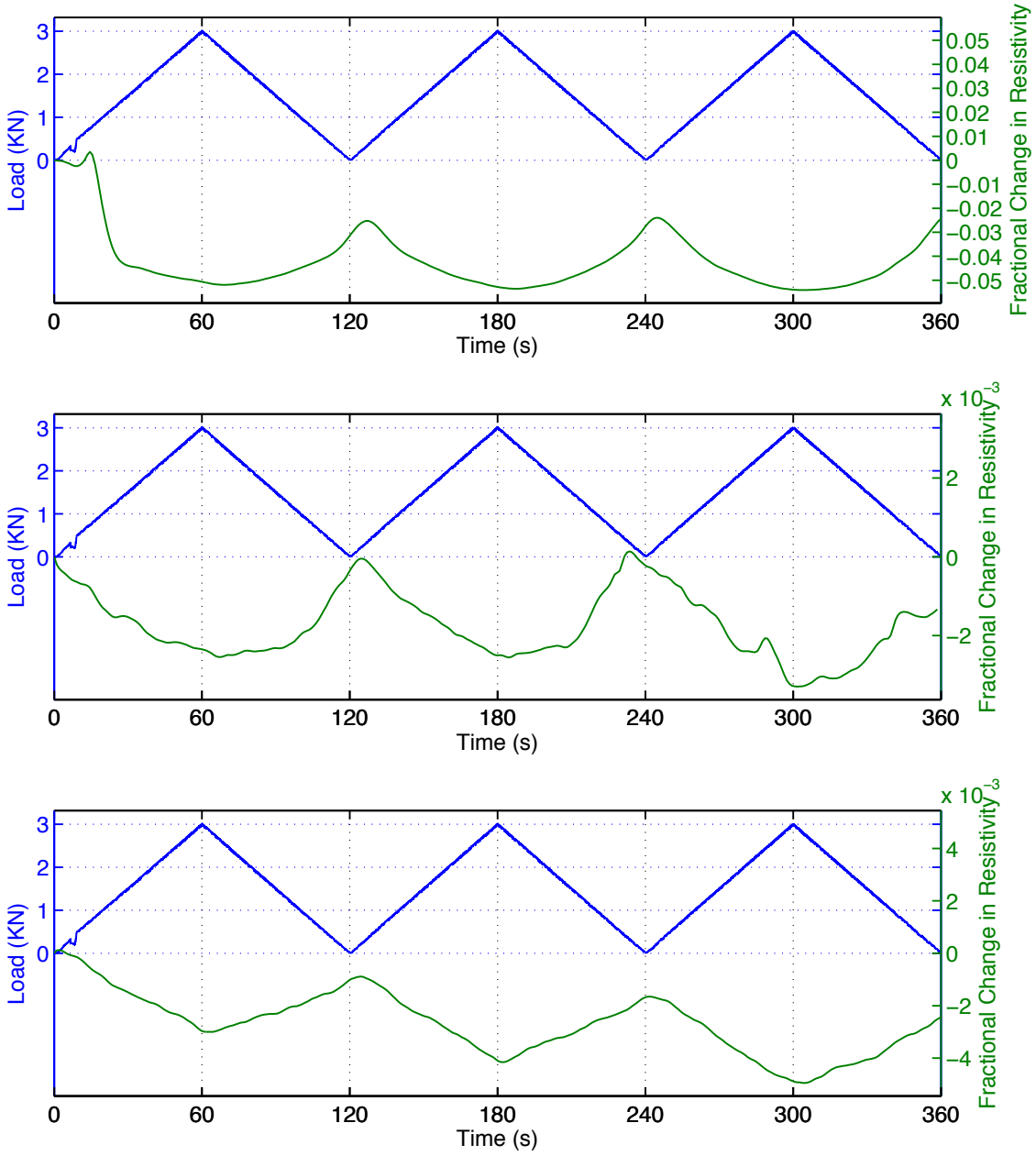

Figure 20. Cyclic compression response of specimens with 7.5% GNPs casted using Method II

CONCLUSIONS

In this study, the effects of GNP concentration, mixing procedure, dispersant type and measurement method on the electrical resistivity of GNP reinforced cementitious composites were investigated. The electrical resistivity of 40 mm × 40 mm × 160 mm prism specimens were measured at different curing ages. The resistivity of specimens increased with the increasing curing age although the rate of increase for each batch was different. A marked decrease in the resistivity was observed at 7.5% GNP concentration for two mixing methods considered in this study, which implies that the percolation threshold might be around that concentration ratio. Although the resistivity measurements for the specimens prepared with each of three mixing methods considered in this study highly affected by the amount of GNPs and the curing age, all mixing methods were effective in producing a conductive mixture at 7.5% GNP concentration ratio. In addition, even though the measurement of the resistivity with different methods such as using internal copper meshes, surface copper tapes or Wenner probe led to different resistivity value, the trend of the change in electrical resistivity values was similar for each measurement technique. The GNP-reinforced mortar specimens exhibited good piezoresistive behavior under cyclic compressive loads when the GNP ratios exceed 5%. However, further investigations are needed to fully characterize the piezoresistive behavior of GNP-reinforced mortars.

RECOMMENDATIONS

Based on the findings of the current study, following recommendations can be made for future research:

- The addition of GNPs with volume ratios below %5 by weight of cement does not increase the conductivity of the mortar significantly. To obtain a self-sensing mortar, the GNP concentration should be over 5% by weight of cement. Further studies with mixtures above 5% GNP concentrations need to be conducted in order to determine the optimal GNP concentration.
- GNP-reinforced self-sensing mortars can successfully be prepared without any special treating procedures such as ultrasonication and chemical (covalent) treatments by following the fabrication methods discussed in this study. However, further investigations are needed to develop a fabrication procedure with reduced mixing time.
- Measuring the resistivity of the mortar specimens using surface electrodes can produce results similar to those obtained through measurements with embedded electrodes. Therefore, the potential of using Wenner probe in resistivity measurements of self-sensing mortars need to be further investigated due to the ease of that measurement technique.

REFERENCES

[1] Chung D. D. L. (2002). "Electrical conduction behavior of cement-matrix composites." *Journal of Materials Engineering and Performance*, 11(2), 194-204.

[2] Chacko R. M., Banthia N., and Mufti A. A. (2007). "Carbon-fiber-reinforced cement-based sensors." *Canadian Journal of Civil Engineering*, 34(3), 284-290.

[3] Han, Baoguo, Siqi Ding, and Xun Yu. (2015). "Intrinsic self-sensing concrete and structures: A review." *Measurement,* 59, 110-128.

[4] Galao O., Baeza F. J., Zornoza E., Garcés P. (2014). "Strain and damage sensing properties on multifunctional cement composites with CNF admixture." *Cement and Concrete Composites*, 46, 90-98.

[5] Wen S., and Chung D. D. L. (2001). "Carbon fiber-reinforced cement as a strain-sensing coating." *Cement and Concrete Research*, 31(4), 665-667.

[6] Chen B., and Liu J. (2008). "Damage in carbon fiber-reinforced concrete, monitored by both electrical resistance measurement and acoustic emission analysis." *Construction and Building Materials*, 22(11), 2196-2201.

[7] Xiao H., Li H., and Ou J. (2011). "Self-monitoring properties of concrete columns with embedded cement-based strain sensors." *Journal of Intelligent Material Systems and Structures*, 22(2), 191-200.

[8] Saafi M. (2009). "Wireless and embedded carbon nanotube networks for damage detection in concrete structures." *Nanotechnology*, 20(39), 395502.

[9] Azhari F., and Banthia N. (2012). "Cement-based sensors with carbon fibers and carbon nanotubes for piezoresistive sensing." *Cement and Concrete Composites*, 34(7), 866-873.

[10] D'Alessandro A., Rallini M., Ubertini F., Materazzi A. L., Kenny J. M., and Laflamme S. (2015). "A comparative study between carbon nanotubes and carbon nanofibers as nanoinclusions in self-sensing concrete." *In Nanotechnology (IEEE-NANO), 2015 IEEE 15th International Conference on. IEEE*, 698-701.

[11] Dusza J., Morgiel J., Duszová A., Kvetková L., Nosko M., Kun P., and Balázsi C. (2012). "Microstructure and fracture toughness of Si_3N_4+ graphene platelet composites." *Journal of the European Ceramic Society*, 32(12), 3389-3397.

[12] Zohhadi N., Aich N., Matta F., Saleh N. B., and Ziehl P. (2015). "Graphene Nanoreinforcement for Cement Composites." *In Nanotechnology in Construction.* Springer International Publishing, 265-270.

[13] Wotring E., Mondal P., and Marsh C. (2015). "Characterizing the Dispersion of Graphene Nanoplatelets in Water with Water Reducing Admixture." *In Nanotechnology in Construction*. Springer International Publishing, 141-148.

[14] Alkhateb H., Al-Ostaz A., Cheng A. H. D., and Li X. (2013). "Materials genome for graphene-cement nanocomposites." *Journal of Nanomechanics and Micromechanics*, 3(3), 67-77.

[15] Du H., and Dai Pang S. (2015). "Enhancement of barrier properties of cement mortar with graphene nanoplatelet." *Cement and Concrete Research*, 76, 10-19.

[16] Tong T., Fan Z., Liu Q., Wang S., and Yu Q. (2015). “Investigation of the Effects of Graphene on the Micro-and Macro-Properties of Cementitious Materials.” *In Structures Congress 2015. ASCE*, 1314-1325.

[17] Dai Pang S., Gao H. J., Xu C., Quek S. T., and Du H. (2014). “Strain and damage self-sensing cement composites with conductive graphene nanoplatelet.” *In SPIE Smart Structures and Materials+ Nondestructive Evaluation and Health Monitoring*. International Society for Optics and Photonics, 906126-906126.

[18] Le J. L., Du H., and Dai Pang S. (2014). “Use of 2D Graphene Nanoplatelets (GNP) in cement composites for structural health evaluation.” *Composites Part B: Engineering*, 67, 555-563.

[19] Li, J., and Kim, J. K. (2007). “Percolation threshold of conducting polymer composites containing 3D randomly distributed graphite nanoplatelets.” *Composites Science and Technology*, 67(10), 2114-2120.

[20] Al-Dahawi A., Ozturk O., Emami F., Yıldırım G., and Sahmaran M. (2016). “Effect of mixing methods on the electrical properties of cementitious composites incorporating different carbon-based materials.” *Construction and Building Materials,* 104, 160-168.